Astro 358/Spring 2012

Galaxies and the Universe

Figures + Tables for Lectures (Feb 16-Mar 6)

Dark Matter in Galaxies

Dark Matter in Spiral Galaxies

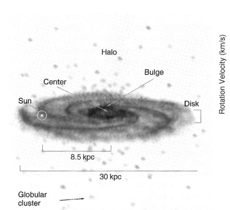

Fig. 1.3. Schematic structure of the Milky Way consisting of the disk, the central bulge with the Galactic center, and the spherical halo in which most of the globular clusters are located. The Sun orbits around the Galactic center at a distance of about 8 kpc

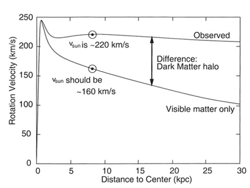

Fig. 1.4. The upper curve is the observed rotation curve $V(R)$ of our Galaxy, i.e., the rotational velocity of stars and gas around the Galactic center as a function of their galacto-centric distance. The lower curve is the rotation curve that we would predict based solely on the observed stellar mass of the Galaxy. The difference between these two curves is ascribed to the presence of dark matter, in which the Milky Way disk is embedded

Flat rotation curve of Milky Way at large radii r , with a circular speed of 220 km/s cannot be accounted for if the total enclosed mass M(r) is made up of only visible mass. It requires a large fraction of M(r) to be dark mattter

(EAC)

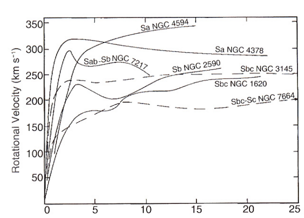

Fig. 3.15. Examples of rotation curves of spiral galaxies. They are all flat in the outer region and do not behave as expected from Kepler's law if the galaxy consisted only of luminous matter. Also striking is the fact that the amplitude of the rotation curve is higher for early types than for late types.

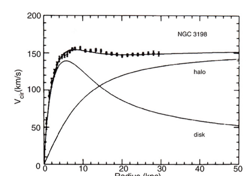

Fig. 3.16. The flat rotation curves of spiral galaxies cannot be explained by visible matter alone. The example of NGC 3198 demonstrates the rotation curve which would be expected from the visible matter alone (curve labeled "disk"). To explain the observed rotation curve, a dark matter component has to be present (curve labeled "halo"). However, the decomposition into disk and halo mass is not unambiguous because for it to be so it would be necessary to know the mass-to-light ratio of the disk. In the case considered here, a "maximum disk" was assumed, i.e., it was assumed that the innermost part of the rotation curve is produced solely by the visible matter in the disk

(EAC)

Dark Matter in Spiral Galaxies

Vera Rubin, with DTM image tube spectrograph attached to the Kitt Peak 84-inch telescope, 1970.vvv

The measured optical velocities from ionized gas clouds of M31 are shown as open and filled circles. Velocities from neutral hydrogen radio observations are shown as filled triangles. Note that velocities remain high far beyond the optical disk.

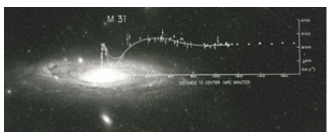

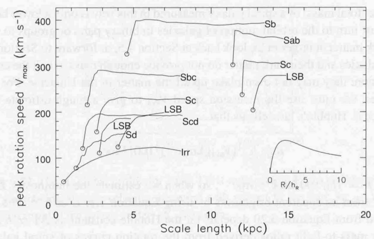

Figure 5.21 Rotation curves for disk galaxies of various types. Open circles show scale length h_R of the stellar disk, and peak rotation speed V_{max} for each galaxy. Curves are plotted in units of R/h_R, to the same horizontal scale as the inset, showing $V(R)$ for the exponential disk (Equation 5.1). LSB denotes a low-surface-brightness galaxy. The measured rotation does not fall as it should if the stellar disk contained most of the mass – A. Broeils, E. de Blok.

(GU)

Dark Matter in the Local Group

The Local Group (Our Local Backyard)

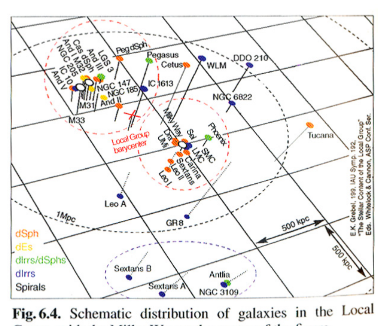

Fig. 6.4. Schematic distribution of galaxies in the Local Group, with the Milky Way at the center of the figure

(EAC)

Local Group (LG) has over 35 galaxies (within a distance of ~1 Mpc of Milky Way)

- No Elliptical or S0 galaxy (recall morphology density relation)
- 3 most luminous members : M31, Milky Way, M33. The first two make up 90% of the total luminosity of LG. M31 is 770 kpc from Milky Way
- Closest neighbors of Milky Way= Sgr I, LMC, SMC
- 15-19 dwarf Sph satellites (more discovered by now) Several dE including M32

Partial list of Members of The Local Group

Table 6.1. Members of the Local Group. Listed are the name of the galaxy, its morphological type, the absolute B-band magnitude, its position on the sphere in both right ascension/declination and in Galactic coordinates, its distance from the Sun, and its radial velocity. A sketch of the spatial configuration is displayed in Fig. 6.4

Galaxy	Type	M_B	RA/Dec.	ℓ, b	D (kpc)	v_r (km/s)
Milky Way	Sbc I-II	−20.0	1830 − 30	0, 0	8	0
LMC	Ir III-IV	−18.5	0524 − 60	280, −33	50	270
SMC	Ir IV-V	−17.1	0051 − 73	303, −44	63	163
Sgr I	dSph?		1856 − 30	6, −14	20	140
Fornax	dE0	−12.0	0237 − 34	237, −65	138	55
Sculptor Dwarf	dSph	−9.8	0057 − 33	286, −84	88	110
Leo I	dSph	−11.9	1005 + 12	226, +49	790	168
Leo II	dSph	−10.1	1110 + 22	220, +67	205	90
Ursa Minor	dSph	−8.9	1508 + 67	105, +45	69	−209
Draco	dSph	−9.4	1719 + 58	86, +35	79	−281
Carina	dSph	−9.4	0640 − 50	260, −22	94	229
Sextans	dSph	−9.5	1010 − 01	243, +42	86	230
M31	Sb I-II	−21.2	0040 + 41	121, −22	770	−297
M32=NGC 221	dE2	−16.5	0039 + 40	121, −22	730	−200
M110=NGC 205	dE5p	−16.4	0037 + 41	121, −21	730	−239
NGC 185	dE3p	−15.6	0036 + 48	121, −14	620	−202
NGC 147	dE5	−15.1	0030 + 48	120, −14	755	−193
And I	dSph	−11.8	0043 + 37	122, −25	790	—
And II	dSph	−11.8	0113 + 33	129, −29	680	—
And III	dSph	−10.2	0032 + 36	119, −26	760	—
Cas = And VII	dSph		2326 + 50	109, −09	690	—
Peg = DDO 216	dIr/dSph	−12.9	2328 + 14	94, −43	760	—
Peg II = And VI	dSph	−11.3	2351 + 24	106, −36	775	—
LGS 3	dIr/dSph	−9.8	0101 + 21	126, −41	620	−277
M33	Sc II-III	−18.9	0131 + 30	134, −31	850	−179
NGC 6822	dIr IV-V	−16.0	1942 − 15	025, −18	500	−57
IC 1613	dIr V	−15.3	0102 + 01	130, −60	715	−234
Sagittarius	dIr V	−12.0	1927 − 17	21, +16	1060	−79
WLM	dIr IV-V	−14.4	2359 − 15	76, −74	945	−116
IC 10	dIr IV	−16.0	0017 + 59	119, −03	660	−344
DDO 210, Aqr	dIr/dSph	−10.9	2044 − 13	34, −31	950	−137
Phoenix Dwarf	dIr/dSph	−9.8	0149 − 44	272, 68	405	56
Tucana	dSph	−9.6	2241 − 64	323, −48	870	—
Leo A = DDO 69	dIr V	−11.7	0959 + 30	196, 52	800	—
Cetus Dwarf	dSph	−10.1	0026 − 11	101, −72	775	—

Table 6.1 EAC

Dark Matter in The Local Group

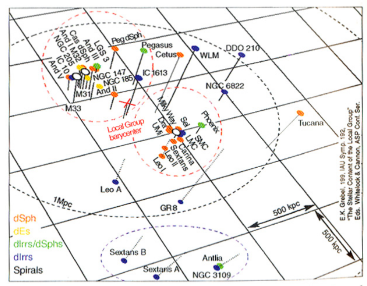

Fig. 6.4. Schematic distribution of galaxies in the Local Group, with the Milky Way at the center of the figure

(EAC)

- Mass of (Milky Way +M31) = 3e12 Mo
- Dark Matter fraction = 96%
- → See class notes for the derivation

Dark Matter in Clusters of Galaxies

Dark Matter in Cluster of Galaxies using Virial Theorem

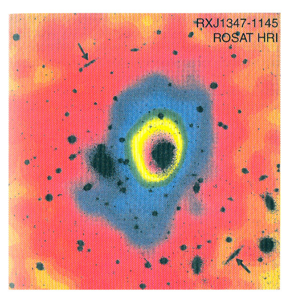

Fig. 6.14. RXJ 1347−1145 is the most luminous galaxy cluster in the X-ray domain. A color-coded ROSAT/HRI image of this cluster, which shows the distribution of the intergalactic gas, is superposed on an optical image of the cluster. The two arrows indicate giant arcs, images of background galaxies which are strongly distorted by the gravitational lens effect

(EAC)

- See in-class notes for applying virial theorem to cluster of galaxies
- Mass of galaxy cluster
  - 3% stars in galaxies
  - 15% in hot gas (T>=10^7 K) located BETWEEN galaxies, and seen in X-ray.. Called the intra-cluster medium or ICM
  - 80% dark matter
- M/L of cluster = 300/h Mo/Lo !!

Using Gravitational lensing to trace mass (of MACHOS, galaxies, cluster of galaxies)

Gravitational lensing from a mass concentration

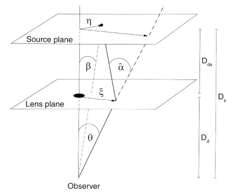

Fig. 2.22. Geometry of a gravitational lens system. Consider a source to be located at a distance D_s from us and a mass concentration at distance D_d. An optical axis is defined that connects the observer and the center of the mass concentration; its extension will intersect the so-called source plane, a plane perpendicular to the optical axis at the distance of the source. Accordingly, the lens plane is the plane perpendicular to the line-of-sight to the mass concentration at distance D_d from us. The intersections of the optical axis and the planes are chosen as the origins of the respective coordinate systems. Let the source be at the point $\boldsymbol{\eta}$ in the source plane; a light beam that encloses an angle $\boldsymbol{\theta}$ to the optical axis intersects the lens plane at the point $\boldsymbol{\xi}$ and is deflected by an angle $\hat{\boldsymbol{\alpha}}(\boldsymbol{\xi})$. All these quantities are two-dimensional vectors. The condition that the source is observed in the direction $\boldsymbol{\theta}$ is given by the lens equation (2.74) which follows from the theorem of intersecting lines

Fig 2.22 EAC: Geometry (3-D view) of a gravitational lensing system.

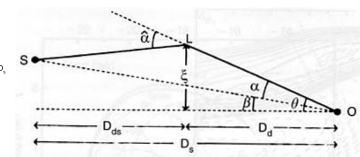

Fig 3.34 EAC: Lens Geometry

- Read Ch 2.5 + 3.8 EAC on gravitational lensing
- See in class-notes for solution to position θ of images for the case where lens is a point mass M and gravitational field is weak

Gravitational lensing of a source by a point mass M

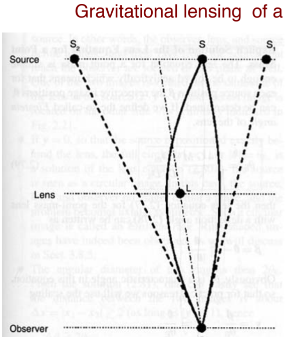

Fig. 2.21. Sketch of a gravitational lens system. If a sufficiently massive mass concentration is located between us and a distant source, it may happen that we observe this source at two different positions on the sphere

Fig 2.25 EAC

See in class-notes for solutions to the position θ of lensed images for a point mass lens, for two cases of β (angular distance of source from line joining observer and lens):

i) β or y >0 : 2 images of opposite side of source (different distances and magnification)
ii) β or y= 0 : Einstein ring

Gravitational lensing of a circular source by a point mass M

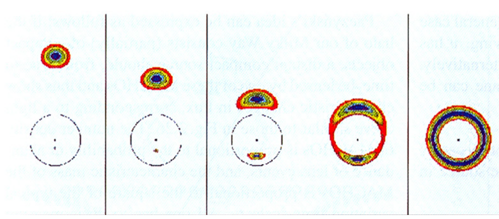

Fig. 2.25. Image of a circular source with a radial brightness profile – indicated by colors – for different relative positions of the lens and source. y decreases from left to right; in the rightmost figure $y = 0$ and an Einstein ring is formed

Fig 2.25 EAC

See in class-notes for solutions to the position θ of lensed images for a point mass lens, for two cases of β (angulardistance of source from line joining observer and lens):

i) β or y >0 : 2 images of opposite side of source (different distances and magnification)
ii) β or y= 0 : Einstein ring

Magnification of a source due to lensing

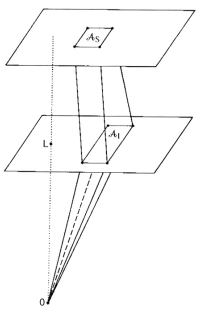

Fig. 2.23. Light beams are deflected differentially, leading to changes of the shape and the cross-sectional area of the beam. As a consequence, the observed solid angle subtended by the source, as seen by the observer, is modified by gravitational light deflection. In the example shown, the observed solid angle $\mathcal{A}_I/D_d^2$ is larger than the one subtended by the undeflected source, $\mathcal{A}_S/D_s^2$ – the image of the source is thus magnified

- Flux of source = surface brightness x solid angle ω
- If the solid angle ω rises due to gravitational lensing, the observed flux is magnified to a larger value than the true source flux
- This is a purely geometrical effect

Fig 2.23 EAC

Low- mass objects as lens (microlensing)

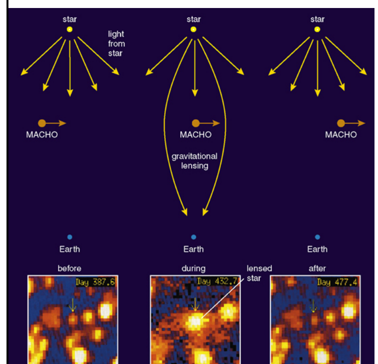

Microlensing : Lens is a low mass object with mass ranging from planets to stars, such as:.

a) Visible objects (hot white dwarfs, stars)

b) MACHOS= massive compact halo objects that are dark e.g., brown dwarfs, planets, dead white dwarfs, neutron stars, low-mass black holes

As light from a bulge star or halo star travels to us, it can be bent by the force of gravity from a passing microlens (e.g., a MACHO) if the latter crosses the light's path.

See in-class derivation showing
- The 2 images (or Einstein ring) are unresolved: see only 1 image
- Flux magnification changes with time: can measure timescale of variability

Searching for MACHOS in our Galaxy via Microlensing

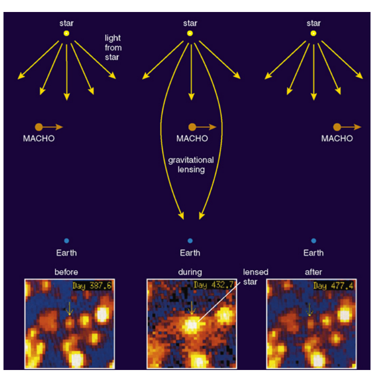

Results: MACHOS make up only a small % f (20%) of the dark matter in the Milky Way.

Galaxies and Galaxy Clusters as Gravitational lens

1) Low-mass lens (microlens) produce 2 images with separation $\Delta\theta$ of order of 10^{-3} arcseconds → 2 images unresolved with current facilities

EFS: What is PSF of ground telescopes with and w/o adaptive optics? And of HST?

2) But lens with mass ~ galaxy mass expected to produce $\Delta\theta$ of order of 1-few arcseconds → see in class-notes for proof

3) Read EAC Ch 3.8 and see in-class notes for how derivation of lens equation for **a point-mass lens with a weak gravitational field** ($\phi \ll c^2$) be expanded to treat the case of **an extended lens with a weak gravitational field** ($\phi \ll c^2$)

4) Lens strength characterized by dimensionless quantity $K(\theta) = \Sigma/\Sigma_{crit}$
-Strong lens has $K(\theta) \gg 1$ at some points : some source positions lead to multiple images
-Weak lens has $K(\theta) \ll 1$ at all points (no multiple images)

Galaxies and Galaxy Clusters as Gravitational lens

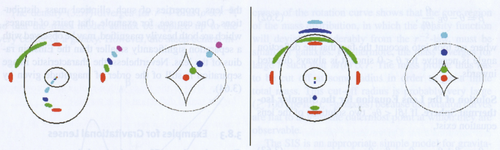

Fig. 3.36. Geometry of an "elliptical" lens, whereby it is of little importance whether the surface mass density Σ is constant on ellipses (i.e., the mass distribution has elliptical isodensity contours) or whether an originally spherical mass distribution is distorted by an external tidal field. On the right-hand side in both panels, several different source positions in the source plane are displayed, each corresponding to a different color. The origin in the source plane is chosen as the intersection point of the line connecting the center of symmetry in the lens and the observer with the source plane (see also Fig. 2.22). Depending on the position of the source, one, three, or five images may appear in the lens plane (i.e., the observer's sky); they are shown on the left-hand side of each panel. The curves in the lens plane are the *critical curves*, the location of all points for which $\mu \to \infty$. The curves in the source plane (i.e., on the right-hand side of each panel) are *caustics*, obtained by mapping the critical curves onto the source plane using the lens equation. Obviously, the number of images of a source depends on the source location relative to the location of the caustics. Strongly elongated images of a source occur close to the critical curves

Galaxies and Galaxy Clusters as Gravitational lens

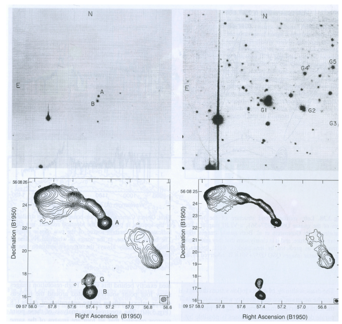

Fig 3.37 EAC

Fig. 3.37. Top: optical images of the double quasar QSO 0957+561. The image on the left has a short exposure time here, the two point-like images A,B of the quasar are clearly visible. In contrast, the image on the right has a longer exposure time, showing the lens galaxy G1 between the two quasar images. Several other galaxies (G2-G5) are visible as well. The lens galaxy is a member of a cluster of galaxies at $z_d = 0.36$. Bottom: two radio maps of QSO 0957+561, observed with the VLA at 6 cm (left) and 3.6 cm (right), respectively. The two images of the quasar are denoted by A,B; G is the radio emission of the lens galaxy. The quasar has a radio jet, which is a common property of many quasars (see Sect. 5.3.1). On small angular scales, the jet can be observed by VLBI techniques in both images (see Fig. 3.38). On large scales only a single image of the jet exists, seen in image A; this property should be compared with Fig. 3.36 where it was demonstrated that the number of images of a source (component) depends on its position in the source plane

Double quasar QSO 0957+561

- First lens system discovered
- 2 images with same redshift z=1.4 and spectral properties, at separation $\Delta\theta$ of 6"
- Lens = Elliptical galaxy + cluster of galaxy at z=0.36

Galaxies and Galaxy Clusters as Gravitational lens

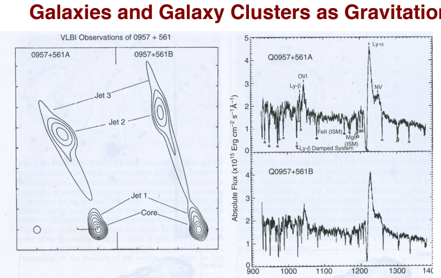

Fig 3.38 EAC

Fig. 3.38. Left: milliarcsecond structure of the two images of the quasar QSO 0957+561, a VLBI map at 13 cm wavelength by Gorenstein et al. Both quasar images show a core-jet structure, and it is clearly seen that they are mirror-symmetric, as predicted by lens models. right: spectra of the two quasar images QSO 0957+561A,B, observed by the Faint Object Camera (FOC) on-board HST. The similari[ty] of the spectra, in particular the identical redshift, is a cle[ar] indicator of a common source of the two quasar image[s]. The broad Lyα line, in the wings of which an Nv line [is] visible, is virtually always the strongest emission line [in] quasars

Double quasar QSO 0957+561

- First lens system discovered
- 2 images with same redshift z=1.4 and spectral properties, at separation $\Delta\theta$ of 6"
- Lens = Elliptical galaxy + cluster of galaxy at z=0.36

Galaxies as Gravitational lens

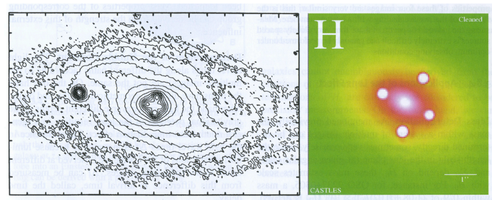

Fig 3.40 EAC

Fig. 3.40. Left: in the center of a nearby spiral galaxy, four point-like sources were found whose spectra show strong emission lines. This image from the CFHT clearly shows the bar structure in the core of the lens galaxy. An HST/NICMOS image of the center of QSO 2237+0305 is shown on the right. The central source is not a fifth quasar image but rather the bright nucleus of the lens galaxy

QSO 2237+0305 (Einstein Cross)

- 4 images with same redshift z=1.72 and spectral properties of a quasar centered on nearby low redshift spiral galaxy (the lens)
- The quasar likely lies exactly behind the lens
- Image have separation $\Delta\theta$ = 1.9", suggesting Einstein radius θ_E= 0.9"

Galaxies and Galaxy Clusters as Gravitational lens

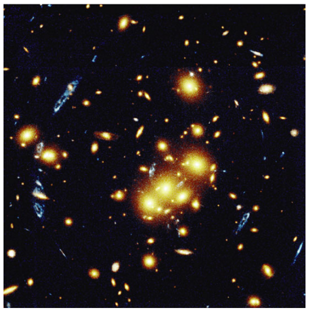

Fig 6.33 b – EAC

now been measured. Bottom image: the cluster of galaxies Cl 0024+17 ($z = 0.39$) contains a rich system of arcs. The arcs appear bluish, stretched in a direction which is tangential to the cluster center. The three arcs to the left of the cluster center, and the arc to the right of it and closer to the center, are images of the same background galaxy which has a redshift of $z = 1.62$. Another image of the same source was found close to the cluster center. Also note the identical ("pretzel"-shaped) morphology of the images

Use gravitational lensing by an intervening galaxy or cluster of galaxies to trace its total (dark+visible) mass

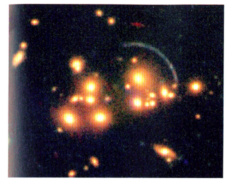

Fig. 6.31. The cluster of galaxies Cl 2244−02 at redshift $z = 0.33$ is the second cluster in which an arc was discovered. Spectroscopic analysis of this arc revealed the redshift of the corresponding source to be $z_s = 2.24$ – at the time of discovery in 1987, it was the first normal galaxy detected at a redshift > 2. This image was observed with the near-IR camera ISAAC at the VLT. Above the arc, one can see another strongly elongated source which is probably associated with a galaxy at very high redshift as well

(EAC)

Fig. 6.33. Top image: the cluster of galaxies A 2218 ($z_d = 0.175$) contains one of the most spectacular arc systems. The majority of the galaxies visible in the image are associated with the cluster and the redshifts of many of the strongly distorted arcs have now been measured. Bottom image: the

Candidates for Dark Matter

Candidates for Dark Matter

Can rule OUT options below for dark matter candidates:

- high and intermediate mass stars: emits UV, optical light
- low mass stars : emit near-IR light
- hot gas : emits X-ray light
- warm gas and dust: emit mid-IR light
- cold gas : emits radio light

Candidates for Dark Matter

Dark Matter

- Baryonic dark matter (made of n and p)
  - MACHOS (Massive Compact Halo Objects)
    - a. Brown dwarfs or failed stars (M/Mo<0.08) and planetary bodies
    - b. Dead white dwarfs
    - c. Black holes, neutron stars
    - d. Extremely low-mass stars
- Non-baryonic dark matter (contains no n or p)
  - Cold Dark matter
    - Massive, slow-moving.
    - Predictions of bottom up or hierarchical formation of structure agrees with observations
    - WIMPS (Weakly Interacting Massive Particles)
      - Likely produced right after Big Bang when Universe was very hot and protons had extreme energies
  - Hot dark matter
    - Fast-moving v→ c
    - Predicts top-down structure formation that disagrees strongly with observations of galaxies, clusters, and superclusters
    - Neutrinos
      - Produced
      - when Universe was very hot soon after Big Bang
      - in nuclear reaction of stars

Leading candidate = Cold dark matter = WIMPS

Bottom-Up or Hierarchical Mode of Structure Formation in CDM models

Cold DM models: structure on small scales form first

Matter particles (p,n,e) have emerged over t=10^{-6}-1s due to symmetry breaking or the excess of matter over antimatter particles

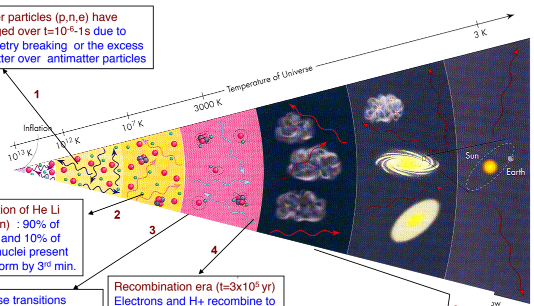

Formation of He Li (t=3 min) : 90% of the He and 10% of the Li nuclei present today form by 3[rd] min.

Universe transitions from radiation-dominated to matter-dominated. (t=3x10^4 yr)

Matter over-densities COLLAPSE ON SMALL SCALES FIRST

Recombination era (t=3x10^5 yr) Electrons and H+ recombine to form neutral H. The photons no longer trapped by e-, travel freely, causing the Universe to change from opaque to transparent. The photons get redshifted to form the present CMB at λ~ 1.2 mm and T=2.7 K

Formation sequence: stars at t=0.05-0.1 Gyr), then proto-galaxies (t=0.3-0.7 Gyr), then clusters and super-clusters form at t>5 Gyr

Observed structures compared to HDM & CDM models

Structures on **small spatial and mass scales (e.g., dwarf galaxies)** are seen **at early epochs** (z~6, age of Universe ~0.9 Gyr)

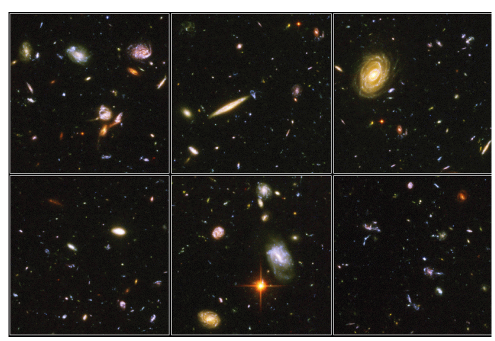

Hubble Ultra Deep Field imaged in 2004 (Credit: NASA/STScI/HUDF home team)

Observed structures compared to HDM & CDM models

Structures **on large scales**, such as galaxy clusters (R~few Mpc) and galaxy superclusters (R~10 Mpc) are frequent at **late epochs** (z<1, age of Univ >5.7 Gyr)

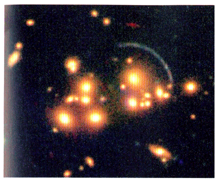

Galaxy cluster with radius ~1.5 Mpc, seen at z=0.33 (age of Universe =9.9. Gyr)

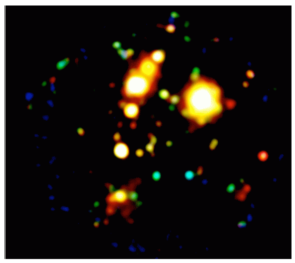

Abell 901/902 supercluster with R~10 Mpc (Xray map)
Made of 3 galaxy clusters in the process of assembling
Seen at z=0.17 (age of Univ =11.4 Gyr)

Characterizing WIMPS with the Large Hadron Collider

Goal of Large Hadron Collider (LHC) in CERN , at Franco-Swiss border is to collide protons and ions head-on, at 99.999999% of the speed of light, at energies ($E=10^{12}$ eV) and temperatures ($T = 10^{16-17}$ K) higher than ever achieved before. These conditions recreate the conditions just after the "Big Bang".

LHC results expected by 2014

It will characterize WIMPS

CDM particles (WIMPS) are leading candidates for dark matter

(Visible + Dark Matter) vs Dark Energy

1) Matter (dark +luminous) exerts an attractive force of gravity that tries to contract the Universe

2) Dark energy
Observations of white dwarf superovae (Type Ia supernovae; standard candles) out to large distances and early times, show that dark energy is causing the expansion of the Universe to accelerate (Nobel Prize 2012)
"a repulsive force or pressure associated with vacuum energy"

3) The competition between matter (both dark and luminous) versus dark energy determines
- the geometry of space (close, flat, open)
- the ultimate fate of the Universe: whether it expands forever or eventually re-collapse

4) Observations show (dark matter + visible matter + radiation) make up only 27% of the total energy density while dark energy makes up a whopping 73%

Radiation like CMB	0.005%
Visible matter :	0.5 %
Baryonic dark matter (e.g., MACHOS)	3.5 %
Non-baryonic cold dark matter (e.g., WIMPS)	24.0%

Total energy density in (dark matter+ luminous matter + radiation)	27.0 %
Total energy density in dark energy	73.0 %